ISSN 0511-5728
The West Indian Journal of Engineering
Vol.43, No.2, January/February 2021, pp.54-68

Flow Induced Vibrations of Oil and Gas Piping Systems: Wall Pressure Fluctuations and Fatigue Life Assessment

Richard Bachoo [a,Ψ], and Jacqueline Bridge [b]

Department of Mechanical and Manufacturing Engineering, Faculty of Engineering, The University of the West Indies, St. Augustine, Trinidad and Tobago, West Indies

[a]Email: Richard.Bachoo@sta.uwi.edu;
[b]Email: Jacqueline.Bridge@sta.uwi.edu

[Ψ] *Corresponding Author*

(Received 12 May 2020; Revised 16 December 2020; Accepted 23 February 2021)

Abstract: *Engineers and analysts primarily rely on the Energy Institute's (EI) Guidelines for the Avoidance of Vibration Induced Fatigue Failure in Process Pipework to determine the possibility of a piping system failing due to flow induced vibration. Whilst the EI Guidelines provides a quantitative measure for the likelihood of failure and gives possible remedial actions, certain key parameters such as the fatigue life cannot be obtained. In this work a procedure for incorporating the underlying wall pressure fluctuations in a finite element model for the purpose of determining the fatigue life of a piping system is provided. Numerical simulations are used to determine the fatigue life for a flowline transporting natural gas at three different flow velocities; 65 m/s, 130 m/s and 170 m/s. The study also experimentally investigates the wall pressure fluctuations associated with single phase flow in a geometrically complex manifold. Extensive wall pressure fluctuation measurements associated with water flowing at 1.6 m/s and air flowing at 3 m/s are presented. It has been shown that owing to the dramatic changes in geometry, the pressure fluctuations associated with a fully developed turbulent flow are significantly greater than that observed at an undisturbed position. Unlike the simple 90^o elbow or mitre bend, the fluctuations within the manifold remain pronounced with no decay in amplitude. Specifically, for the case of water flowing at 1.6 m/s it is observed that the mean square pressure along the manifold falls within the range of 113 dB and 116 dB, whilst the undisturbed position had a mean square pressure of 104 dB. For the case of air flowing at 3 m/s, the mean square pressure ranged between 101 dB and 107 dB throughout the entire manifold.*

Keywords: *Fatigue Assessment, Flow Induced Vibration, Piping vibrations, Piping manifold, Random Vibration, Wall Pressure Fluctuation*

1. Introduction

The upstream and downstream oil and gas industries are major contributors to the Gross Domestic Product (GDP) of many Caribbean territories. One major asset that both upstream and downstream facilities have in common are the vast networks of process piping. Industrial plants, by their nature, transport fluids from one point to another and piping networks facilitate this core function. It is often the case that piping is responsible for 25% - 35% of the material in a processing plant, consumes 30% - 40% of the construction labor, and utilises 40% - 48% of the engineering man-hours in design, fabrication, and installation (Peng and Peng, 2009; Wu et al., 2018).

Flow induced vibration (FIV) is a common source of excitation in piping systems and occurs when the fluid being transported is forced to negotiate a change in geometry such as a piping bend or tee. The corresponding change in momentum creates strong pressure gradients beneath the turbulent boundary layer and results in a broadband excitation source. In particular, FIV can induce large fluctuating deflections and bending stresses on adjacent small bore piping connections (SBCs) potentially resulting in sudden and catastrophic failure (Garrison, 1998).

Several researchers have studied the effects of flow induced vibrations in simple and complex piping systems. Tunstall and Harvey (1968) experimentally investigated the flow in a mitre bend using flow visualisation. The work illustrated that flow downstream the bend was characterised by flow separation and a randomly switching swirling action. Bull and Norton (1981) later showed that the flow separation in the mitre bend acts as an excitation source that generates non-propagating pressure fluctuations, plane wave propagation and acoustically induced travelling waves. Bull and Norton (1981) further determined the associated wall pressure fluctuations of air with velocities between 0.2 to 0.5 Mach. In a later study, Norton and Bull (1984) reported the wall pressure fluctuations in other types flow obstructions: 90^o radius bends, 45^o mitred bends, a fully opened butterfly valve and a partially opened gate valve.

With respect to two-phase flow, Riverin (2006) measured the spectral density of the forces generated at a 90º elbow and impacting tee for different volumetric ratios of an air-water mixture. Belfroid et al. (2016) investigated the forces generated in large 6-inch diameter piping with a long radius bend when high velocity single phase and multiphase fluids were transported. Peltier and Hambric (2007) used a Reynolds Average Navier Stokes technique to predict the surface pressure power spectra in a 90º long radius bend. In a later study (Hambric et al., 2010) used the wall spectra information to calculate the structural and acoustical noise sources emitted by the piping.

Although it is evident that a wide range of research on FIV has been reported, the Energy Institute's Guidelines for the Avoidance of Vibration Induced Fatigue Failure in Process Pipework (Energy Institute 2008) is currently the only standard used to screen industrial process piping systems for potential failure due to flow induced vibrations. A major limitation of the guidelines (Energy Institute, 2008) is that it only provides crude estimates of the likelihood of failure and not detailed information such as fatigue life, which are critical for Designers and Engineers seeking to optimise the dynamic behavior of a piping system.

In this work a finite element based methodology is proposed to determine the fatigue life of a piping system subjected to flow induced vibration. The method incorporates the effects of the spatially distributed wall pressure fluctuations due to flow separation within the pipe. The efficacy of the method is demonstrated by performing numerical simulations on a flowline transporting high velocity flow streams. Comparisons are made between the results of the detailed finite element model and that of the recommendations proposed by the EI Guidelines (Energy Institute, 2008) for multiple flowrates.

Oil and gas piping networks are often routed to a piping manifold where flow is channeled and diverted to multiple locations. In the literature, flow induced vibration in piping manifolds have received little attention. Most of the studies to date, regarding piping manifolds, have focused on the hydraulic aspects of the flow as opposed to flow induced vibration and wall pressure fluctuations (Pigford et al., 1983; Bajura, 1971; Graber, 2010). As part of the work presented herein, extensive wall pressure fluctuations measurements on a complex piping manifold transporting single phase water flowing at 1.6 m/s and air at 3 m/s are presented. The key physical differences between the flow characteristics of the manifold compared to turbulent flow in a simple 90º bend are identified and discussed.

2. General Approach to Assessing Piping Vibrations

The methodology for undertaking a vibration assessment using the EI Guidelines (Energy Institute, 2008) consists of three stages. In the first stage, the section of the plant to be analysed is specified. Industrial plants often segment their entire operations into separate facilities based on the particular process or function taking place.

In the second stage, quantitative assessments of the mainline piping for each type of excitation identified in Stage 1 are carried out. The EI guidelines from the Energy Institute (2008) provides clear information on the parameters required for the flow induced vibration screening assessment. The input parameters are usually obtained from the PIDs, piping isometrics and knowledge of the operating conditions. Equations are provided to determine a parameter called the mainline Likelihood of Failure (LOF). The value of the LOF guides analysts on the actions that are required to minimise failure due to fatigue. The guidelines propose four categories of actions based on the LOFs as explained in Table 1.

Table 1. Proposed Recommendations based on the Energy Institute's Guidelines for the Avoidance of Vibration Induced Fatigue Failure in Process Pipework for Mainline Piping

Likelihood of failure	Recommendations
LOF< 0.3	The likelihood of failure of the mainline and SBCs are low. The guidelines, however, still advises that a field survey should be executed to ensure that the conditions specified in the assessment were achieved on the field.
0.5 > LOF ≥ 0.3	The likelihood of failure of the mainline is low, however, an additional assessment on the SBCs **should** be done. A field survey is recommended.
1 > LOF ≥ 0.5	The mainline **should** be redesigned or resupported to lower the LOF to an acceptable level. Small bore connections **shall** be assessed. Another alternative is to undertake experimental vibration measurements or detailed analysis to predict if the fatigue life of the piping and its branch connections are acceptable. A field survey is recommended.
LOF ≥ 1	The mainline **shall** be redesigned or resupported to lower the LOF to an acceptable level. Experimental vibration analysis or detailed modeling can also be used to predict if the fatigue life is acceptable. A field survey is recommended.

Source: Abstracted from Energy Institute (2008)

Notably, a separate assessment for SBCs on the mainline is suggested when the LOF is greater than 0.5. The SBC assessment is the third stage of screening, and considers the span-wise and cross-sectional geometry of the SBC, the type of fitting used to connect the SBC to the mainline, the number of valves on the SBC and the thickness of the mainline piping. This assessment produces a new set of LOFs with a separate set of actions as shown in Table 2.

The flowchart in Figure 1 illustrates how the screening process may be implemented for a typical industrial facility. A key feature in the recommendations includes a field visit to examine the mainline and small bore connections. Such examinations are necessary to ensure that the input data used in the screening analysis matches that which is on the field. For instance, often analysts may take credit for a piping-support only to realise that the pipe has lifted off its initial positon during

the construction phase leaving the support completely inactive.

Table 2. Proposed Recommendations based on the Energy Institute's Guidelines for the Avoidance of Vibration Induced Fatigue Failure in Process Pipework for Small Bore Piping

Likelihood of failure	Recommendations
LOF< 0.4	The SBC has a low likelihood of failure. A field survey is still recommended.
0.7 > LOF ≥ 0.4	The SBC **should** be redesigned or resupported to lower the LOF to an acceptable level. Experimental vibration analysis or detailed modeling can also be used to predict if the fatigue life is acceptable. A field survey is recommended.
LOF ≥ 0.7	The SBC **shall** be redesigned or resupported to lower the LOF to an acceptable level. Experimental vibration analysis or detailed modeling can also be used to predict if the fatigue life is acceptable. A field survey is recommended.
LOF ≥ 1	The mainline **shall** be redesigned or resupported to lower the LOF to an acceptable level. Experimental vibration analysis or detailed modeling can also be used to predict if the fatigue life is acceptable. A field survey is recommended.

Source: Abstracted from Energy Institute (2008)

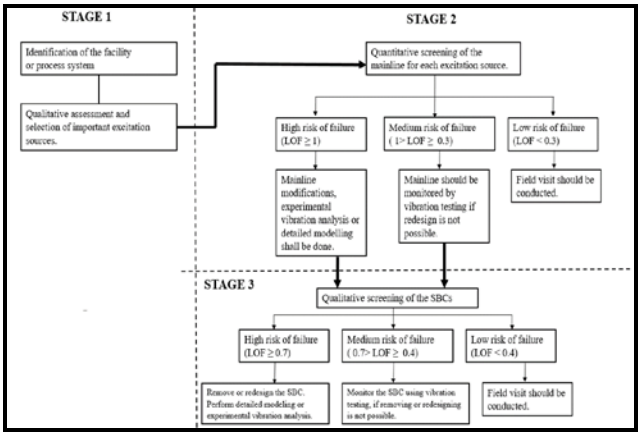

Figure 1: Flowchart illustrating the Qualitative and Quantitative Procedures of the Energy Institute's Guidelines for the Avoidance of Vibration Induced Fatigue Failure in Process Pipework

Source: Abstracted from Energy Institute (2008)

Engineers performing a field examination should pay particular attention to:

1. damaged and compromised piping supports and clamps,
2. the visible movement of lines and small bore connections,
3. the integrity of weldolets and sockolets connecting the SBC to the mainline piping, and
4. impact noises or tonal sounds and locate where they are emanating from.

Critical locations identified from the screening study combined with the points, piping spans or small bore connections that display symptoms of vibration issues from the field examinations are often then measured by using appropriate instrumentation and suitably qualified personnel. One other recommendation the EI guidelines alludes to in situations where the LOFs of the mainline or small bore are relatively large; is that a detailed analysis of the system can be conducted (Energy Institute, 2008). The EI guidelines offers this as a recommendation in recognition that a detailed analysis would provide a more accurate and informative description of the piping system's response. Such output information may include the frequencies of the natural modes that are excited, the output response in terms of velocity, stress and strain, and perhaps most importantly the fatigue life of the piping.

Inherently, a detailed analysis lowers the risk of implementing solutions to piping problems that are overly conservative or unknowingly risky. No information regarding the procedure to conduct detailed analyses for the specific excitation mechanisms are given in the EI guidelines, and in many cases upstream and downstream gas companies seek the help of specialists to perform such simulations.

3. Flow Induced Vibration

3.1 Wall Pressure Fluctuations and FIV

The response of a piping system can only be predicted if the sources of excitation are known. In the case of piping systems having a turbulent flow which is forced to navigate sharp geometric changes, one source of excitation is the underlying wall pressure fluctuation. As illustrated in Figure 2 the wall pressure fluctuation on the underside of the piping can be due to the occurrence of:

1. a naturally existing turbulent boundary layer generated on the internal piping walls,
2. low frequency plane waves traversing the piping circuit,
3. higher frequency acoustical modes, and
4. localised fluctuations occurring within the proximity of an internal disturbance due to flow separation and pressure gradients.

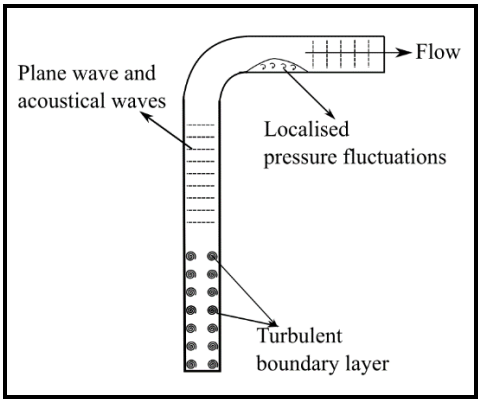

Figure 2. Sources of Wall Pressure Fluctuations due to Flow Induced Turbulence

The unsteady random nature of a fully developed turbulent flow results in pressure fluctuations in straight length pipes with no upstream internal obstruction of flow. These wall pressure fluctuations are the minimum excitation levels in a piping systems and forms a baseline signature to further understand the relative contribution of other excitation sources. The wall pressure excitations in straight piping with turbulent flow are statistically uniform along both the circumference and length of the piping system (Norton, 2003).

The acoustic field in a closed loop piping system behaves as an acoustic transmission line and is characterised by the generation, transmission, propagation and radiation of sound from the piping walls. This process can occur over the entire audible frequency range (0-20 kHz). At the lowest frequencies where the wavelengths generated are large compared to the cross sectional dimensions of the pipe only plane waves propagate and the system can be considered one-dimensional. At any instant in time, the acoustic parameters such as displacement, velocity and pressure are constant on any plane perpendicular to the direction of wave travel for a propagating plane wave. The one-dimensional acoustic theory of ducts dictate that plane wave propagation can occur at certain frequencies which are dependent on the working fluid, geometry and configuration of the piping (Jaconbsen, 2013).

3.2 Detailed FIV Analysis of a Natural Gas Flow-line with a Blind Tee

Natural gas flowlines are used on offshore platforms to connect the wellhead to a main production header or separator. Depending on the nature of the subsurface well, the flowline can transport mainly single phase gas at the early points in its history and multiphase liquid-gas mixtures at the latter end. Figure 3 shows the top view of a typical horizontal flowline that is connected on one end to the wellhead and on the other end to a pressure vessel or separator. The two major piping discontinuities on the flowline are the 90º blind tee and the small bore branch connection. A detailed finite element analysis model of the flowline will be used to determine the fatigue life of the critical locations on the mainline piping and small bore connection due to FIV. The internal diameter of the mainline piping is 78 mm and the thickness is 5.49 mm, whilst the internal diameter of the SBC is 26.7 mm with a similar thickness of 5.49 mm. A valve of mass 1.0 kg is connected to the end of the SBC. The span lengths of the mainline connection and SBC are as shown in Figure 3.

3.2.1 Wall Pressure Spectrum

The excitation mechanism for flow-induced vibration are the wall pressure fluctuations. The non-dimensional axial and circumferential wall pressure fluctuations provided by Bull and Norton (1981) due to a mitre bend can be used for the case of a blind tee since both fittings are similar geometrically. The non-dimensional power spectral densities (PSDs) and its variation along the axial length of the mitre are replicated in Figure 4.

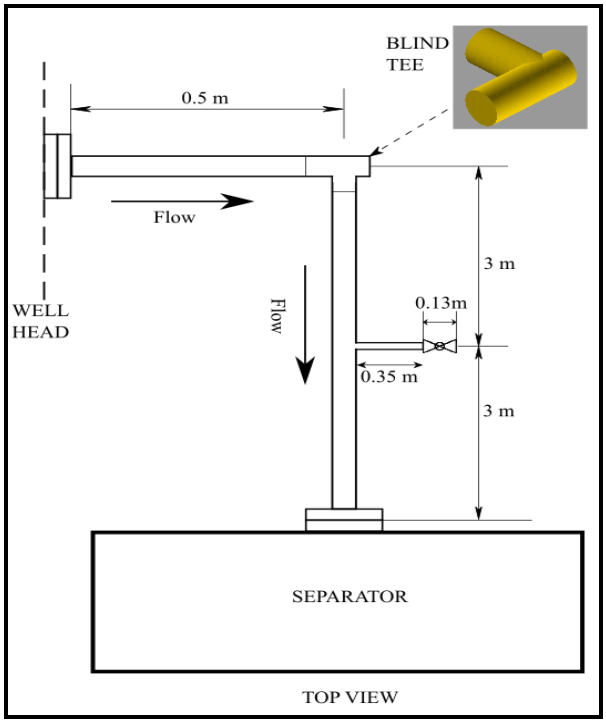

Figure 3. Flowline Connecting the Wellhead to the Separator on an Offshore Platform

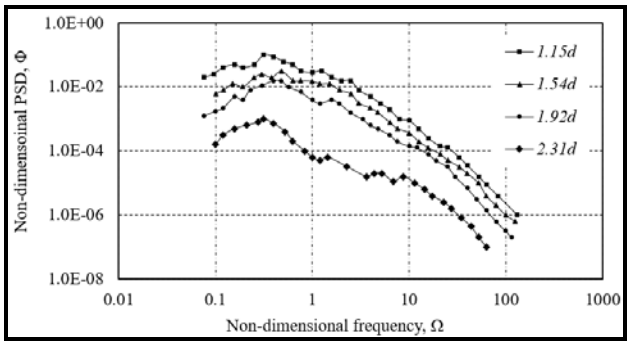

Figure 4. Non-dimensional Wall Pressure PSDs along the Axial Direction of a Mitre Bend

The non-dimensional PSD (Φ) is related to the dimensional or actual excitation PSD (ϕ) by the equation,

$$\Phi = \frac{4\phi}{\rho_f^2 U_o^3 a}, \tag{1}$$

where ρ_f is the density of the fluid, U_o is the centre line velocity of the flow, and a is the internal radius of the piping. Similarly, the non-dimensional frequency (Ω) is related to the radian frequency (ω) by the equation,

$$\Omega = \frac{\omega a}{U_o}. \tag{2}$$

Norton and Pruiti (1991) discussed how the non-dimensional PSD for the mitre can be scaled to obtain approximations for the actual wall pressure PSDs for different velocity flows and piping diameters. By comparing the magnitude of the PSDs, it is observed from the Bull and Norton (1981) study, that wall pressure fluctuations upstream of the mitre have a negligible contribution to flow induced vibration. A similar observation is made for the wall pressure fluctuations beyond 2.31 times the piping diameter downstream the mitre.

3.2.2 Finite Element Model of a Flowline

The finite element method is a useful tool for analysing the free and forced vibration characteristic of systems with complex geometry and loading conditions. A continuous structure is discretised into a contiguous set of elements and the equation of motion is given in the following matrix form:

$$[M]\ddot{q}+[C]\dot{q}+[K]q=\mathrm{F}(t) \tag{3}$$

where M, C and K are the mass, damping and stiffness matrices respectively. The term q is the displacement vector, $(\cdot)$ and $(\cdot\cdot)$ are the first and second derivatives with respect to time respectively and F(t) is the load vector. Owing to the complexity of large scale piping systems, finite element analysis is used to solve most dynamic problems and the basis for determining the response has its foundation in Eq. (3) above.

In this work a finite element model (FEM) was generated in the commercial software Ansys APDL 18.0 for the flowline in Figure 3. A total of 18,577 two dimensional SHELL281 elements were used with gradual refinement at the location of the mitre, small bore connection and end boundaries. The piping material was carbon steel having a density of 7,800 kg/m^3, a Young's Modulus of 200 GPa and a Poisson ratio of 0.3. The ends of the piping were treated as fixed owing to the large stiffness (and weight) of both the wellhead and separator. The valve at the end of the SBC was modelled as the same internal diameter and thickness of the small bore piping, however, the density of this piping-run was adjusted so that an equivalent mass of 1kg, similar to the mass of the valve, is obtained. The damping ratio of metallic piping is typically taken as 1% (Cremer et al., 2001; Mossou, 2003).

The first step to describing the response of the piping due to random excitation requires that the modes of vibration and the associated natural frequencies be calculated. This requires that the eigenvalue problem,

$$-\omega_n^2[M]\vec{q}+[K]\vec{q}=\vec{0}, \tag{4}$$

be solved. In Eq. (4), $\omega_1,\omega_2,\omega_3\ldots$ are the natural frequencies with the corresponding eigen vectors, $\vec{q}_1,\vec{q}_2,\vec{q}_3\ldots$. A modal analysis using the Subspace algorithm within Ansys extracts all modes and natural frequencies between 0.1 to 500 Hz for the entire piping system.

Conducting the modal analysis is necessary to apply the modal superposition technique to solve the inherent random vibration problem. Modal superposition characterises the piping response by linearly combining the undamped modes, usually within the frequency band of interest. Mathematically, this is represented as:

$$q(r,t)=\sum_{n=1}^{\infty}\psi_j(r)q_j(t) \tag{5}$$

where r is a spatial position vector, $\psi_j(r)$ is the undamped mode shape of order j and $q_j(t)$ is the modal coefficient. Therefore prior to conducting the random vibration or spectral analysis in Ansys 18.0, the modes are first expanded.

Random vibration theory shows that the response cross-spectral density $S_{qq}(r_1,r_2,\omega)$ between two displacements $q(r_1,t)$ and $q(r_2,t)$ can be determined for a distributed excitation with cross spectral density, $S_{pp}(r_1,r_2,\omega)$ from the expression

$$S_{qq}(r_1,r_2,\omega)=\int_R\int_R H^*(r_1,s_1,\omega)H(r_2,s_2,\omega)S_{pp}(s_1,s_2,\omega)\mathrm{d}s_1\mathrm{d}s_2\ , \tag{6}$$

where $H(r_1,S_1,\omega)$ is the frequency response function for the response at position r_i due to a unit harmonic input at position s_i (Newland, 2012). In Ansys 18.0, a random spectral analysis was used to impose the power spectral densities of the underlying distributed pressure fluctuations. The correlations between pressure fluctuations from one point to the other decreases exponentially with axial and circumferential distance and can be considered to be uncorrelated (Durant, 2000). In conventional Finite Element packages such as Ansys APDL, uncorrelated pressures cannot be directly applied to a structure. Consequently, the wall pressure spectral densities must be transformed into uncorrelated nodal force spectral densities; a process described in Maymon (2008).

Bull and Norton (1981) gave the third-octave-band-averaged wall pressures at discrete axial locations and the magnitude of the PSDs decreased as the distance from the mitre increased. To use this information within the context of an FEM framework, the non-dimensional PSDs are converted to actual wall pressure PSDs for the fluid density and velocities of interest. In this study, the density of the natural gas flowing through the pipe is ρ_f = 4 kg/m^3 with a dynamic viscosity (μ) of 10^{-5} Pa.s. Three separate flow velocities, U_o = 65m/s, 130 m/s and 172 m/s are considered. For each velocity the four non-dimensional curves in Figure (4) are transformed to four dimensional wall pressure PSD curves at the locations, 1.15d, 1.54d, 1.92d and 2.31d downstream the mitre; where d is the diameter of the pipe and the units of the PSD is now in Pa^2/Hz.

Since the diameter of the flowline and velocities of the fluid are approximately equal to that used in Bull and Norton (1981) the scaled values are also approximately the same. The dimensionalised wall pressure PSDs are

also third-octave-band-averaged values. One can approximate the time-averaged root mean square pressure in a particular frequency band, for a particular location, as

$$P_{rms} = \sqrt{\phi(f_c)\Delta f} \tag{7}$$

where $\phi(f_c)$ is the transformed wall pressure fluctuation (in Pa^2/Hz) at the centre frequency f_c and Δf is the third octave frequency bandwidth. Some lower centre frequencies and bandwidths are shown in Table 3 for different third octave bands.

Table 3. Third Octave Frequency Bands

Band	Bandwidth, Δf (Hz)	Centre frequency, f_c (Hz)
1	5.2	22.4
2	6.5	28.3
3	8.3	35.6
4	10.4	44.9
5	13.1	56.6
6	16.5	71.3
7	20.8	89.8
8	26.2	113.1
9	33	142.5
10	41.6	179.6
11	52.4	226.3
12	66.0	285.1
13	83.2	360.0

Exact knowledge of the wall pressure fluctuations at every axial position is impractical to obtain experimentally. Therefore, for the purpose of tractability we can assume that the time-averaged root mean square pressure P_{rms}, as obtained from Bull and Norton (1981), is constant both circumferentially and longitudinally in the region between measurement points. The justification for this assumptions is as follows: (1) it is inherently conservative since the amplitudes decrease with increasing distance from the mitre, (2) the number of positions measured by Bull and Norton (1981) in the axial direction is sufficiently refined to demonstrate a clear monotonic smooth trend in wall pressure fluctuations along the length of the pipe, and (3) Bull and Norton (1981) has shown for a wide range of operating conditions there is little to no variation of the PSD in the circumferential positions at any particular axial location.

The proposed regions for which the pressure is constant in the axial and circumferential directions are shown in Figure 5. Each of the four regions is associated with their respective PSD curve in Figure 4. It follows, an equivalent total force (F_{tot}) acting on a particular region in a specific frequency band (Δf) can be determined by multiplying the pressure, P_{rms} by the associated surface area it acts upon. This total force is now divided by the number of nodes in the region to produce an equivalent set of radially directed nodal forces (F_n). The nodes must be axisymmetrically distributed about the longitudinal axis of the pipe to permit an even distribution of pressure for each of the four regions.

A uniform PSD value for the force excitation acting on each node in a particular frequency band can then be obtained as $F_n^2/\Delta f$. Therefore, the power spectral density in terms of a nodal forcing function, where all the forces are uncorrelated within the excitation region $a < z \leq 2.31d$ is achieved, and the problem can be processed in the finite element software.

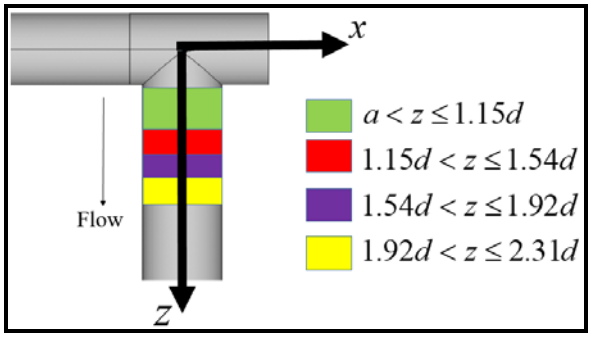

Figure 5. Regions of Constant Wall Pressure Fluctuation

3.2.3 Piping Response and Fatigue Analysis

The finite element solution generates the power spectral density (PSD) of the displacement at any node on the piping system according to Eq. (6) where the input excitation spectral density must be known. From the displacement PSD, the velocity and bending stress PSDs are important quantities that can be subsequently derived. Integrating the velocity PSD over the entire frequency band of interest leads to the temporal mean square velocity

$$v_{rms}^2(r) = \int_{\Delta\omega} S_{\dot{q}\dot{q}}(r,\omega)\, d\omega \tag{8}$$

which is a parameter that is used directly in several criteria to determine if the vibration levels are acceptable in a piping system (Moussou, 2003).

Since the piping is subjected to variable amplitude loading, a cumulative damage fatigue model is needed to determine the fatigue life of the system. The SN curve for the piping material is given by

$$N_F S^m = K, \tag{9}$$

where N_F is the number of cycles to failure, for a constant amplitude stress range S. The terms K and m are the fatigue strength coefficient and fatigue strength exponent respectively; both terms can be obtained from standards, such as BS7608 Guide to Fatigue Design and Assessment of Steel Products (BSI, 2014) and the American Bureau of Shipping's Guide for Fatigue Assessment of Offshore Structures (ABS, 2003). In this study, $K = 1.08(10^{14})$ and $m = 3.5$ as recommended for steel welded butt joints (Wirsching, 2006).

Due to its simplicity and wide range of application, Miners cumulative damage rule is the most prevalent model used to determine the damage fraction *D*, due to variable amplitude loading. The rule is given by:

$$D = \frac{1}{K}\sum_{i}^{M} n_i S_i^m \tag{10}$$

where n_i is the number of cycles corresponding to the stress range S_i, and M is the number of stress ranges in the spectrum. When D is equal to unity, the cumulative damage is at 100% and the material fails. Experimentally, analysts obtain stress time histories and use techniques such as Rainflow counting to determine the number of cycles for specific stress ranges and subsequently use Eq. (10) to determine the damage fraction (Lee et al. 2005).

In analytical models, however, the damage fraction is often calculated in the frequency domain using the stress PSD. Dirlik's method is commonly used for calculating the cumulative damage based on the stress PSD from a narrow-band Gaussian process (Dirlik, 1985). Ragan (2007) provides a thorough review of the process involved in using Dirlik's method. The probability distribution function of the stress range (p(S)) in the Dirlik combines two Rayleigh and one exponential distribution functions,

$$p(\mathrm{S}) = \frac{\frac{D_1}{Q}\mathrm{e}^{-Z/Q} + \frac{D_2 Z}{R^2}\mathrm{e}^{-\left(Z^2/2R^2\right)} + D_2 Z\mathrm{e}^{-\left(Z^2/2\right)}}{2\sqrt{m_0}}. \tag{11}$$

The terms in Eq. (11) are calculated as follows,

$$D_1 = \frac{2\left(x_m - \gamma^2\right)}{1+\gamma^2},\quad D_2 = \frac{1-\gamma-D_1+D_1^2}{1-R},\quad D_3 = 1-D_1-D_2,$$

$$Q = \frac{1.25\left(\gamma - D_3 - D_2 R\right)}{D_1},\qquad R = \frac{\gamma - x_m - D_1^2}{1-\gamma-D_1+D_1^2}$$

$$\mathrm{Z} = \frac{S}{2\sqrt{m_0}},\ x_m = \frac{m_1}{m_0}\sqrt{\frac{m_2}{m_4}},\ \text{and}\ \gamma = \frac{m_2}{\sqrt{m_0 m_4}}.$$

The n^{th} moment of the spectral density is given by $m_n = \int_0^\infty f^n P_s(f)\mathrm{d}f$, where P_s is the stress PSD. The expected damage fraction in time T seconds is given by,

$$E[D] = \frac{T}{K}E[P].E\left[S^m\right], \tag{12}$$

where $E\left[S^m\right] = \int_0^\infty S^m p(S)\mathrm{d}S$, and $E[P] = \sqrt{\frac{m_4}{m_2}}$ is the expected number of peaks in the spectrum. Therefore, the time T when E[D] is unity represents the time to failure. A program, written in Matlab, is used to implement the Dirlik and calculate the estimated fatigue life of the piping system in Figure 3.

3.3 Assessment using EI Guidelines and Comparison with Detailed Analysis

Analysts screening the flowline in Figure 3 would generally follow the flowchart shown in Figure 6 to determine the LOF values from the EI Guidelines (Energy Institute, 2008). Table 1 provides guidance as to the recommended actions. The fluid viscosity factor (*FVF*) is only dependent on the dynamic viscosity of the natural gas and in this case the *FVF* = 0.1. The EI Guidelines first considers the means by which a span length of piping is supported, and then classifies it into one of four types: Stiff, Medium Stiff, Medium and Flexible (Energy Institute, 2008). The span length is defined as the distance between two fixed or partially fixed supports. As one moves from the Stiff to Flexible classifications the fundamental natural frequencies of the piping segment decreases.

Equations which are functions only of the outer diameter and span length are used to determine which classification is appropriate. For the case of the flowline, the span length is therefore 6.5 m and the calculation from the EI Guidelines (per Table 2-1 page 50) indicates that it falls into the Medium region (Energy Institute, 2008). A flow induced vibration factor (F_v) then needs to be calculated (as per Table 2-2 page 51 of the EI Guidelines). This factor depends on the span length classification, outer diameter and thickness of the piping. For the system under consideration, the F_v = *10857*. One important point to note is that up until now in the screening analysis the momentum of the fluid was not considered; that is neither the density or the velocity. Specifically, the stiffness classification and flow induced vibration factor are only dependent on the geometry of the piping. The LOF as shown in Figure 6 only incorporates momentum of the fluid at the last stage of the calculation.

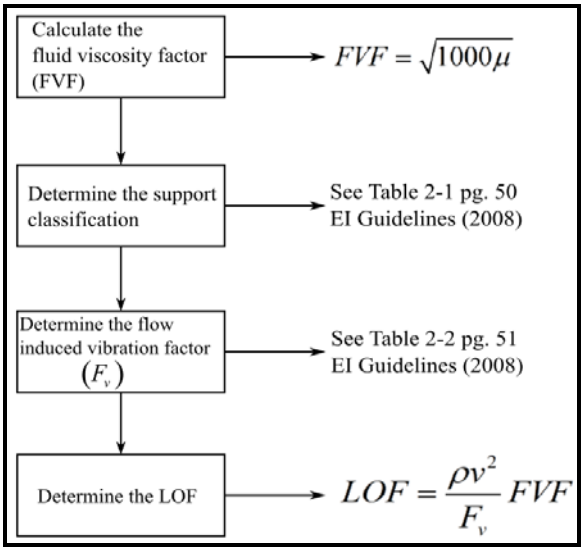

Figure 6. Screening Procedure for FIV
Source: Based on Energy Institute (2008)

The resulting LOFs of the mainline for the three separate flow rates considered are as shown in Table 4. Alongside the LOFs are the fatigue life in years

predicted for the most stressed location on the piping system as obtained from the detailed analysis in Section 3.2 of this work.

Table 4. Results from the Screening Process and Detailed Finite Element Analysis for the Flowline

Velocity (m/s)	Likelihood of failure of mainline as per EI Guidelines	Likelihood of failure of SBC as per EI Guidelines	Fatigue life of most stressed position on the flowline with SBC/ Years to failure	Fatigue life of most stressed position on the flowline without SBC/Years to failure
65	0.09		665	
130	0.62	0.70	31	792
170	1.10	0.70	9	282

Source: Based on the Energy Institute (2008)

At 65 m/s the LOF is at its lowest value of 0.09 and from the EI Guidelines (Energy Institute, 2008), as per Table 1, only a field survey is required. The small bore connection is also deemed safe. The detailed finite element simulation indicates that the critical location is at the junction between the mainline and the small bore connection (see Figure 7). This position gave a fatigue life of 665 years. Typically, offshore piping is designed for a service life ranging between 10-40 years (Guo et al., 2005). Therefore, the FE model's prediction is in agreement with that of the EI Guidelines (Energy Institute, 2008).

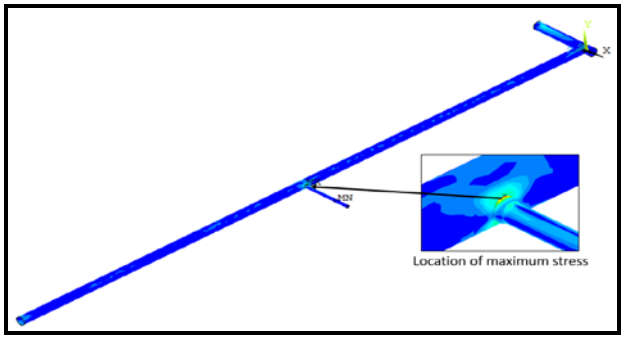

Figure 7. Detailed FEM shows that the largest stress occurs at the junction between the SBC and mainline piping. FEM Model show for U_o = 65m/s

Figure 8 shows the stress PSD at the critical location. The flow velocity for this case is U_o = 65m/s. The largest peak in the stress PSD occurs at 84 Hz which corresponds to a resonant mode where the SBC has a large displacement relative to the mainline piping. At 130 m/s the LOF is 0.62; and requires that either the mainline be resupported, redesigned or detailed analysis conducted. A screening on the small bore connection is also required in line with the procedures given on pages 73-80 in the EI Guidelines (Energy Institute, 2008). This screening process calculates one LOF based on the geometric configuration of the SBC and another separate LOF based on the location of the SBC on the mainline piping. It chooses the minimum value of the LOF citing that "both a poorly placed and poorly designed SBC need to be present to have a high LOF".

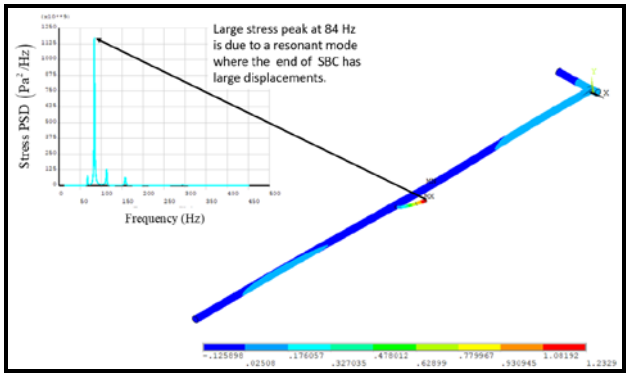

Figure 8. Stress PSD for the Critical Location on the Flowline

The SBC LOF is calculated as 0.7 for the mainline flow of 130 m/s, and therefore falls into the riskiest category as shown in Table 2. The guidelines as per the information calls for the SBC to be removed, redesigned or a detailed analysis conducted. The detailed analysis shows that the most stressed location is again the junction between the mainline and the small bore connection. The stress, however, has intensified significantly and the fatigue life has decreased to 31 years.

The piping is often designed for a maximum of 40 years, the recommendation from the EI Guidelines is correct with respect to the SBC and it should be removed or redesigned. Upon removing the SBC from the mainline the flow of 130 m/s was once again simulated through the piping and the largest stress was found to be at the edge of the flowline where it was fixed to the wellhead (see Figure 9). This critical point gave a fatigue life of 792 years. Therefore, the EI guidelines is conservative in recommending that the mainline be redesigned or resupported.

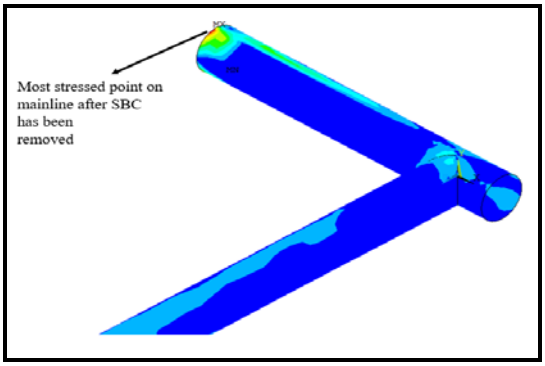

Figure 9. Most Stressed Location on Mainline Piping after Removal of the SBC

At 170 m/s the LOF is 1.1; and falls within the most severe classification in Table 1. The mainline is required to be resupported, redesigned or detailed analysis conducted. The LOF of the SBC, which is required to be calculated, is determined to be 0.7 as well. Hence, as in the previous case the guidelines call for the SBC to be removed, redesigned or a detailed analysis to be conducted.

The detailed analysis shows that the most stressed location at the junction between the mainline and the small bore connection has intensified even more. The fatigue life has now decreased to just 9 years. The recommendation from the EI Guidelines regarding the SBC is once again correct (Energy Institute, 2008). After removing the SBC, the mainline once again had its largest stress located at the edge of the wellhead and a fatigue life of 282 years was calculated. This illustrates that even when the LOF is greater than one, the suggested action for the mainline is too conservative.

One drawback of the EI Guidelines' screening process for FIV is that it fails to take into consideration the orientation of the SBC (Energy Institute, 2008). Consider the case where the SBC is located at the same axial position along the length of the flowline but rotated to lie in the vertical plane as shown in Figure 10. Simulations for the three flow velocities show that although the most stressed location is still at the junction between the SBC and the maninline (see Figure 11), the stress magnitudes have been reduced.

Table 5 shows the fatigue lives for a flowrate of 65 m/s, 130 m/s and 170 m/s are 1951 years, 143 years and 30 years. It is important to note that the LOFs of neither the mainline or SBC have changed because of the rotation of the SBC. It is appropriate for the lowest and highest flow velocities in their recommendation, but is conservative for a flow of 130 m/s (Energy Institute, 2008).

Rotating the SBC is one action that can be taken to reduce the stress levels of the SBC in this particular case. In many situations, however, the physical space may not be available to execute such a change and an alternative modification is required. This challenge is particularly relevant to Brownfield projects where other additional piping routes may already exist in close proximity to the area of interest.

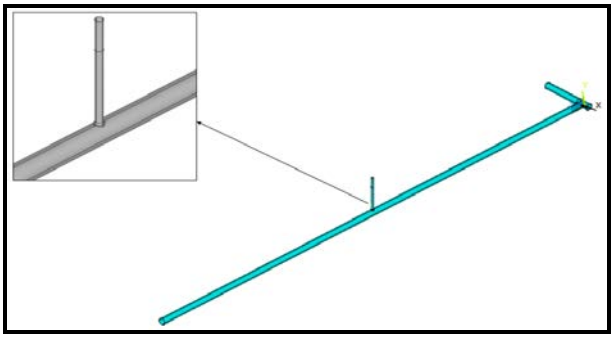

Figure 10. Vertically Oriented SBC on Mainline Piping

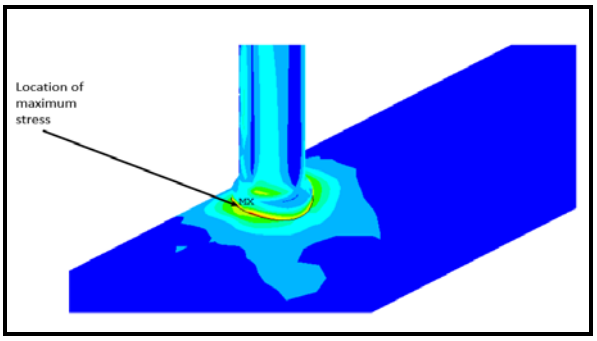

Figure 11. Largest Stress Point on Flowline with a Vertical SBC

Table 5. Results from the Screening Process and Detailed Finite Element Analysis for the Flowline with a Vertical SBC

Velocity (m/s)	Likelihood of failure of mainline as per EI Guidelines	Likelihood of failure of SBC as per EI Guidelines	Fatigue life of most stressed position on the flowline with SBC/ Years to failure
65	0.09		1951
130	0.62	0.70	143
170	1.10	0.70	30

Source: Based on Energy Institute (2008)

The use of an external clamp is a second option that can be used to restrain a SBC from vibrating excessively thereby reducing the stresses at its junction. The clamps are often bolted around the mainline piping and then connected to the end of the SBC, thus providing the constraint. Engineers are advised not to restrain SBCs from any other position other than its mainline, as the effects of thermal expansion may cause the mainline to move independently with respect to the constrained end of the SBC, resulting in large stresses being induced at its junction.

For the horizontal small bore under study a clamp with lengths shown in Figure 12 is used to reduce stress levels at the junction. The clamp is made of a hollow tube steel section with inner radius 0.01 m and thickness 7 mm. The material properties are taken to be the same as the steel piping. The clamp is incorporated in the detailed FE model using BEAM188 elements.

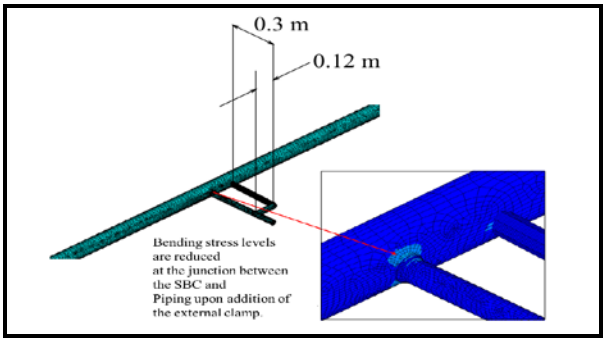

Figure 12. Reducing the Vibration of an SBC by Clamping it to the Mainline

Simulations are then carried out for the flow of 130 m/s and 170m/s, respectively. The largest stress on the piping systems still occurred at the junction of the SBC and mainline, however, the reduced stress PSD resulted in a fatigue life of 142 years for the 130 m/s flow and 44 years for the 170 m/s flow. This represents a 35-year increase in the lifespan for the higher flow rate and a 111-year increase for the lower flowrate. Both SBCs are, therefore, now within acceptable limits.

4. Piping Manifolds

4.1 Wall Pressure Fluctuations in a Piping Manifold

The flow mechanism and pressure fluctuations in a piping manifold are dependent on the piping geometry, flowrate, and intrinsic properties of the fluid. A series of experiments have been carried out to determine the wall pressure fluctuations in a specific piping manifold. A schematic of the test rig is shown in Figure 13. The manifold studied can be deconstructed into three major geometric components: A. The impacting tee, B. The 90º branched tee and C. The 90º radius bend. Each of these geometric configurations have received independent attention from a considerable number of researchers as discussed in the preceding sections. It also known that each of the aforementioned configurations have unique flow patterns and pressure fluctuations which may also change as a flow regime transitions from single phase to multiphase mixtures.

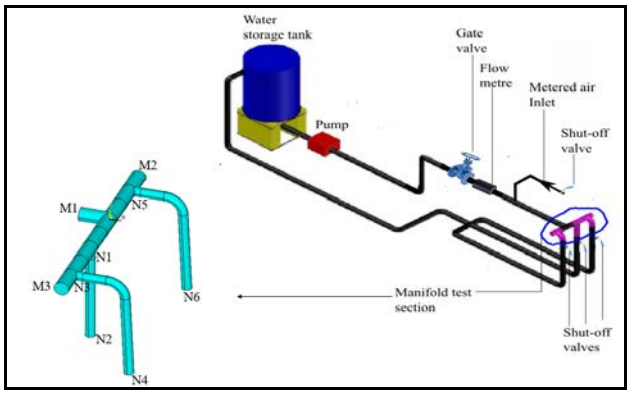

Figure 13. Experimental Test Rig to Investigate the Wall Pressure Fluctuations in Piping Manifolds

The test rig was designed to channel water at ambient temperature from a large storage tank to the manifold test-section. A single impeller Aurora 1070 centrifugal pump pushes water through the piping which has an inner diameter of 77.93 mm and a thickness of 5.49 mm. Water flows through a fully opened gate valve and GPI TM-300F turbine metre before it enters the manifold. A WIKA Type 232.34 pressure gauge was installed to measure the water inlet pressure before entry to the manifold. The internal piping diameter remains the same dimension from the pump outlet to the test manifold inlet, and as a result, there are no upstream disturbances of the fluid prior it entering the manifold.

The test inlet and the distribution channel of the manifold (M1-M2-M3) have a diameter and thickness of 77.93 mm and 5.49 mm, respectively, which is the same as the upstream mainline piping. The ends, M2 and M3, of the distribution channel are closed off using a 3-inch (76.2 mm) nominal diameter hemispherical cap designed according to the standard ASME B16.9 (ASME, 2001). The distribution channel splits the flow into three separate piping channels each having an internal diameter of 52.5 mm and thickness 3.91 mm. The leg N1-N2 is a straight run of pipe directed vertically downwards whilst the legs N3-N4 and N5-N6 both exit on the horizontal plane and are then directed vertically downward. Both the N3-N4 and N5-N6 legs contain a long radius elbow as specified in ASME (2001) with an internal diameter 52.5 mm and thickness 3.91 mm.

Each outlet leg has a ball valve with similar internal radius which can be used to prevent flow through the associated leg. The outlet ball valves are labelled BV1-BV3 for ease of reference. The material for the upstream piping and fittings as well as the test-manifold were all fabricated from carbon steel. All flanges and fittings were welded to the main piping using full penetration butt-welds. The piping downstream the ball valves BV1-BV3 were fabricated from galvanised steel. The downstream piping acts as the return line to the tank and has an internal diameter of 52.5 mm. A range of supports (not shown in the diagram) were placed at several locations to reduce the static stresses on the piping as well mechanical vibrations of the rig. The specific lengthwise dimensions of the manifold and the measurement positions are shown in Figure 14.

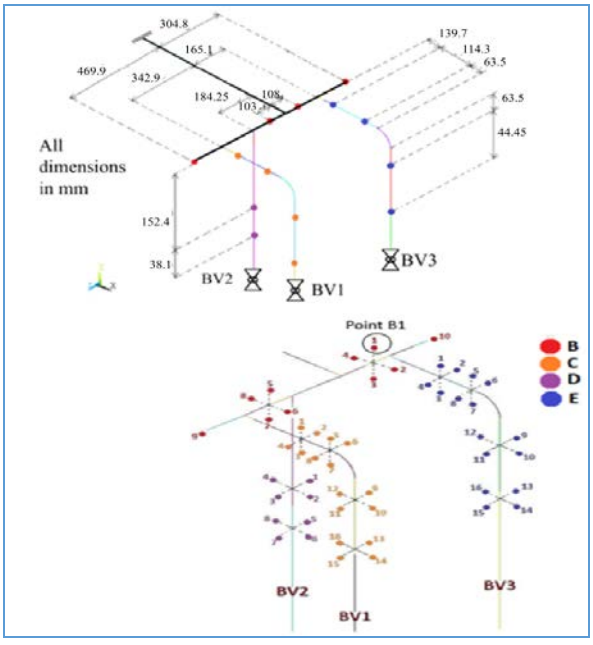

Figure 14. Measurement Locations and Labelling Scheme

In order to measure the underlying wall pressure in the piping manifold, three separate PCB S113B28 pressure sensors were used. At each position along the length of the piping, four measurements were taken at the 0º, 90º, 180º and 360º angles. Two additional points at the centre of each end cap on the manifold were also measured as well a point 15 diameters just downstream the pump to provide a baseline pressure fluctuation for the undisturbed turbulent flow. The undisturbed point is given the notation AX1 from this point on. To accommodate all the measurement points, a total of 51 holes were drilled and tapped such that each sensor can be threaded into place. Owing to the large number of measurement points a colour coded legend is proposed in Figure 14. For instance, the point B1 represents a measurement taken at point 1 on the red dot (circled in diagram).

Specialised bushings were designed for the pressure sensors to be flush mounted with the inside wall of the pipe. The pressure sensors are connected to a multi-channel Kistler Type 5134 power supply. An integrated low-pass filter of 1,000 Hz was used to process the signal prior to sampling. The voltage obtained from the pressure sensors was sampled by a National Instruments NIUSB 6009 analog to digital converter (ADC). An in-house data acquisition program created in National Instruments LabView was used to control the ADC which collected data at a sample rate of 5,000 Hz for two minutes. The two-minute duration was deemed sufficient since the mean square averages were asymptotic after this period.

The test rig (see Figure 13) also incorporated a branch connection that enabled compressed air to be transported through the test manifold. The side branch made of galvanised steel had an internal diameter and thickness of 15.8 mm and 7.11 mm, respectively. Pressurised air from a Kellog 452TV compressor located far upstream of the mainline pipeline was used to investigate the flow of single phase air. A needle valve was added to the line to control the flow of the incoming air into the test manifold. and a check valve and ball valve were located on the branch connection to prevent reverse flow and permit shutting the air on or off respectively. To measure the incoming air-pressure a Wika pressure gauge was used, whilst to measure the air flow a Hedland Flow Meter H771A-150 was included. Since the water storage tank is opened to atmosphere, the air that flows into the tank (unlike the water) never recirculates.

Observing the test rig in its entirety, one can recognise that by closing the air shut-off valve and needle control valve, the air to the manifold is stopped. Upon opening the gate only single phase water passes through the manifold. Similarly, by closing the gate valve and opening the air-line ball valve and needle valve only single phase air passes through the manifold. Evidently, simultaneously opening the gate vale and air valves allows a multiphase mixture to flow through. One can then recognise that by controlling the positions of the gate valve and needle valve along with the outlet manifold ball valves BV1-BV3, the test rig facilitates a wide range of single phase and multiphase flow conditions in several different scenarios.

4.3 Experimental Results and Analysis

Power spectral densities of the wall pressure fluctuations are presented for the following inlet flow conditions:

- Single phase water with an inlet velocity 1.6 m/s and a Reynolds number of 108000.
- Single phase air with an inlet velocity 3 m/s and a Reynolds number of 15844.

Figures 15 and 16 show an example of the variations of the wall pressure fluctuations along the distribution channel and the outlet legs of the manifold for the fully formed turbulent flow of water. On each graph, the PSD of the wall pressure for the undisturbed position (AX1) is also included for comparison.

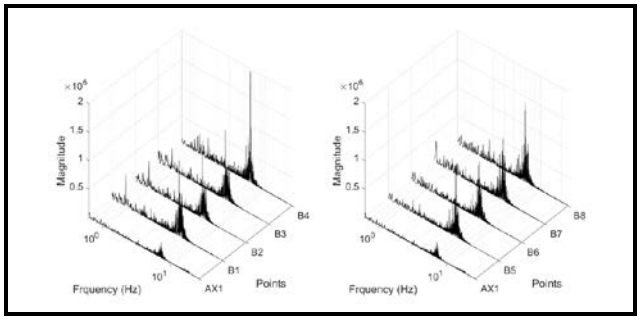

Figure 15. Wall Pressure Fluctuation of Water Flowing at 1.6m/s for Points AX1-B9

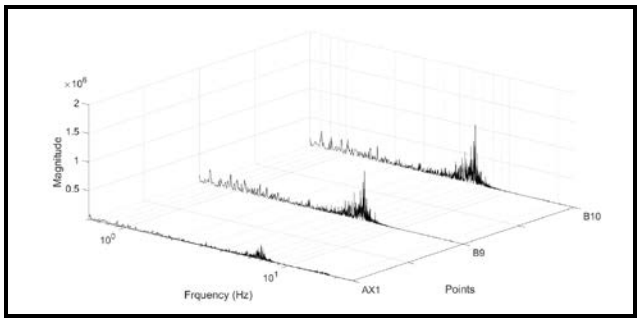

Figure 16. Wall Pressure Fluctuation of Water Flowing at 1.6m/s for Points B9-B10

It is generally observed that the amplitudes in the distribution channel and outlets of the manifold are larger than that of the undisturbed position (AX1). The amplitude of the PSD for all points on the entire manifold are small at the lowest frequencies but show a clear increase between the frequency band of approximately 4-8 Hz with a distinct peak occurring at approximately 6 Hz. Beyond 8 Hz, the amplitudes for all points decrease to negligible levels. The peak within the

region of 4-8 Hz is due to the summation of the baseline straight pipe turbulence, a low frequency plane wave and localised flow disturbances. The negligible amplitudes at the higher frequencies indicate that the high frequency acoustic waves were not excited in this piping system. In systems where the velocities and Reynolds numbers are relatively low, similar results have been reported by several authors (Riverin and Pettigrew, 2007; Wang et al., 2002; Tanaka et al., 2016). The position B4 recorded the largest peak and was greater than the undisturbed position by approximately 17 dB. The time averaged mean square pressure levels for each location is calculated and shown in Figure 17.

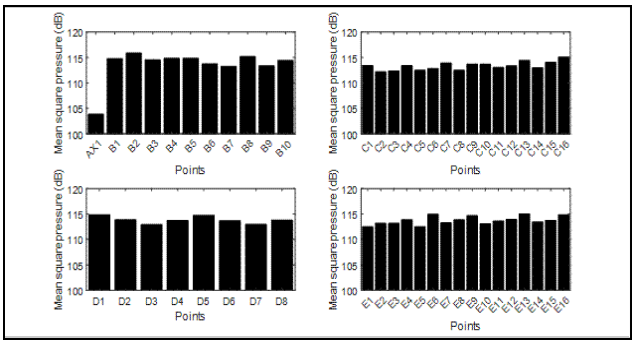

Figure 17. Mean Square Pressure Levels across all Points on the Manifold for Single Phase Water

By analysing the mean square pressure for each point it is observed that all points on the manifold have a mean square value between 113 dB and 116 dB. This is significantly higher than the undisturbed position, which has a mean square pressure of 104 dB. One can therefore conclude that since the baseline wall pressure of the straight pipe is significantly smaller in magnitude than that of the manifold, it must be the case that the contribution of the plane wave propagation and localised turbulent pressure fluctuations contribute significantly more to the wall pressure than the turbulence in the straight piping. It is also clear that these pressure fluctuations are strong enough to propagate through the entire manifold as there is no noticeable attenuation of the mean square pressures along the axial direction of the distribution piping straight through to the outlet piping legs. The variation in pressure fluctuations for the circumferential points at a particular location is also minimal.

Figures 18 and 19 show similar variations of the wall pressure fluctuations along the manifold for single-phase air. The shape of the wall pressure spectrum is similar to that of single phase water. The band of large amplitude pressure has, however, now shifted to be between 0.8 Hz and 2 Hz. Generally, the largest peak occurs at approximately 1.2 Hz. The mechanism which causes these increased pressure levels include non-propagating turbulent disturbances, plane wave propagation and to a much lesser extent; the turbulence associated with the straight piping.

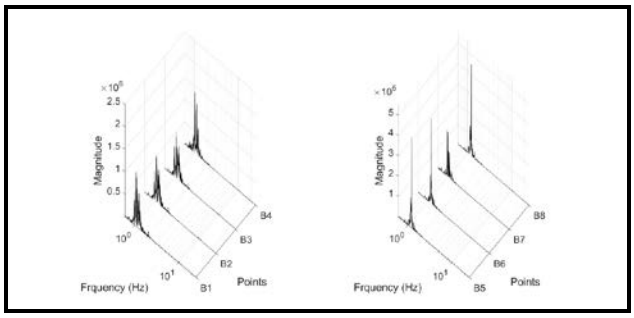

Figure 18. Wall Pressure Fluctuation of Air Flowing at 3m/s for Points B1-B8

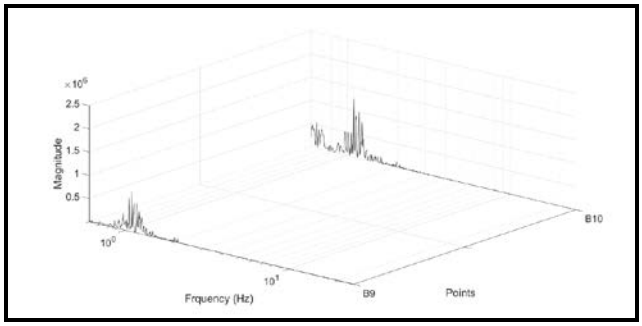

Figure 19. Wall Pressure Fluctuation of Air Flowing at 3m/s for Points B9-B10

A three-dimensional finite element model generated with the commercial finite element software Ansys APDL is used to predict the natural frequencies of the plane waves in the piping system when air is present. The density of air is taken as 1.225 kg/m^3 and the speed of sound in air as 343 m/s. The element type selected is Fluid30. The piping starts at the closed gate valve and ends at the point where the fluid enters the inside of the tank filled with water; both ends are treated as a large impedance mismatch. The branch connection for the inlet air is also included with its entry pressure of 345 kPa. A total of 1,692,975 elements are used for the simulation (see Figure 20). The fundamental natural frequency is calculated to be 2 Hz which is in close proximity to the experimentally observed 1.2 Hz. The mode shape also indicates that the oscillations take the form of propagating plane waves. The model also predicts a number of other plane wave acoustic modes at increasing frequencies, however, similar to the case of water these were not excited due to the relatively low inlet velocity.

The mean square wall pressures are also calculated for the points on the manifold as air passes through the system as shown in Figure 21. Typically, the values lie between 101 dB and 107 dB which shows that there is more variation between measurement points for the case

of air as opposed to water. Similar to the case of water, however, the pressure fluctuations do not attenuate with distance along the manifold and remain relatively large. The variation in pressure fluctuations for the circumferential points at a particular location are observed to be more pronounced compared to the case of water for all the output legs. In certain cases, two points on the same circumferential plane may vary from 4 dB to as high as 6 dB.

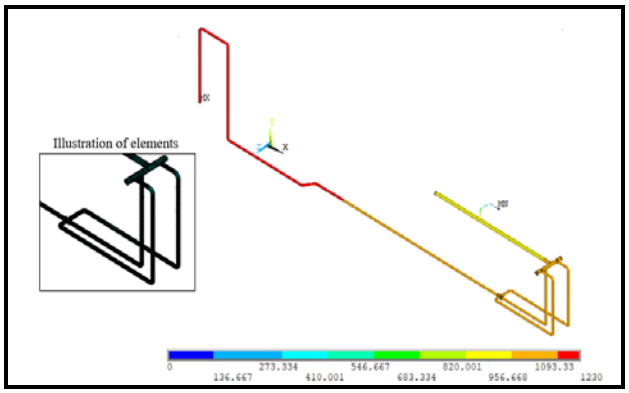

Figure 20. Plane Wave Acoustic Mode at 2 Hz for Air Volume in the Piping System

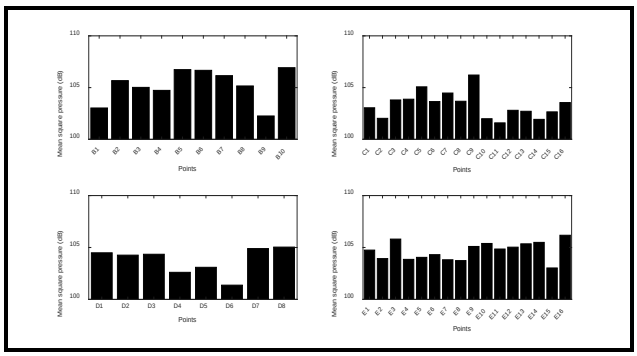

Figure 21. Mean Square Pressure Levels across all Points on the Manifold for Single Phase Air

5. Conclusions

The assessment of piping vibrations in oil and gas processing plants is a compulsory activity required to ensure that the structural integrity of a piping system is not compromised. In the preceding sections, a method to incorporate the random wall pressure excitations within the context of a finite element model to determine the fatigue life at critical locations is described. A specific industrial example of a high velocity gas stream transported through a flowline with a single SBC is used demonstrate the procedure involved. A comparison is made between the results of the detailed finite element model and that of the recommendations by the EI Guidelines for different flowrates.

In general, it is observed that the EI Guidelines is conservative in its recommended actions for the mainline piping. Finite element simulations show that for a range of flowrates the mainline piping stress levels result in fatigue lives that are much greater than the standard design life of 40 years. Conversely, it is also observed that the EI Guidelines generally provided the correct recommended actions for the SBC. Finite element simulations showed that in cases where the fatigue life of the small bore was less than 40 years, the EI Guidelines recommended that it be resupported or removed.

Although, the EI Guidelines recommends taking corrective action for small bore connections prone to failure, it cannot quantitatively evaluate the effectiveness of the change. In this work it is also demonstrated how the finite element model can be used to quantify the increase in fatigue life by taking two corrective actions on the small bore: (1) changing the orientation of the SBC and (2) adding a piping clamp between the mainline and the SBC.

The importance and complexity of the piping manifold in oil and gas industries are discussed. Specifically, the lack of research into the role that wall pressure fluctuations play in generating flow induced turbulence in a piping manifold is highlighted. In this study, the wall pressure fluctuations for a complex piping manifold is investigated for single-phase water flowing at 1.6 m/s and air at 3 m/s separately. Extensive dynamic wall pressure measurements are taken at numerous axial and circumferential points along the manifold. The spectral content of the wall pressures for the case of water indicates that the amplitudes are significantly larger within the manifold compared to an undisturbed upstream position. The increase in wall pressure fluctuations is due to the propagation of a plane wave and localised turbulent action.

Similar observations are made for the case of air flow where finite element simulations are used to validate the presence of a dominating acoustic plane wave. The temporal mean square pressure levels are also calculated and compared across all points on the manifold for both fluids. For the case of water, the pressure levels for each position generally lie within 113 dB - 116 dB whereas for the case of air they lie within 101 dB - 107 dB. Therefore, the pressure pulsations in the manifold are intense enough to propagate throughout the entire manifold, as there is no noticeable attenuation along the axial direction of the distribution piping or the outlet piping legs. In terms of future experimental work on the manifold, it is necessary to investigate the pressure fluctuations at higher flowrates. In this way, the contribution of higher order acoustic modes to flow induced vibration may be obtained.

The results and analysis presented in this study have been limited to single-phase fluid flow. It is often the case, however, that the fluid being transported in industrial pipes are multiphase, consisting of both gas and liquids. Multiphase fluid flow is far more complex

than single-phase flow primarily because the flow regime depends on the velocity of the constituent phases. For instance, Mandhane et al. (1974) produced a widely used flow pattern map that distinguishes between the stratified, bubble, annular and slug flow regimes. The EI guidelines suggests that a multiphase fluid can be treated similar to that of a single-phase fluid upon calculating the equivalent density and equivalent velocity of the mixture (Energy Institute, 2008). This is a crude assumption and is yet to receive scrutiny on its range of validity.

A number of recent studies have also indicated that for multiphase flow in piping systems, the underlying power spectral density changes as the gas to liquid volumetric ratio changes (Belfroid et al., 2016; Riverin et al., 2006). This will also lead the dynamic response of the process piping system to behave differently compared to single-phase flow. Therefore, although the inclusion of multiphase fluid flow is beyond the scope of this study, incorporating such effects is the next reasonable step forward.

References:

ABS (2003), *Guide for Fatigue Assessment of Offshore Structures*, American Bureau of Shipping, Houston, TX.

ASME (2001), *ASME B16.9: Factory-Made Wrought Buttwelding Fittings*, American Society of Mechanical Engineers, New York

Bajura R.A. (1971), "A model for flow distribution in manifolds", *Journal of Engineering Power*, Vol.93, No.1, pp.7-12

Belfroid, S.P.C., Nennie, E., and Lewis, M. (2016), "Multiphase forces on bends – Large scale 6-inch experiments", In: *SPE Annual Technical Conference and Exhibition. Society of Petroleum Engineers*, Dubai World Trade Centre Dubai, UAE, September, 26-28

BSI (2014), *BS 7608: 2014. Guide to Fatigue Design and Assessment of Steel Products*, British Standards Institution, London

Bull, M.K., and Norton, M.P. (1981), "On the hydrodynamic and acoustic wall pressure fluctuations in turbulent pipe flow due to a 90o mitred bend", *Journal of Sound and Vibration*, Vol.76, No.4, pp.561-586.

Cremer, L., Heckl, M., and Petersson, B.A.T. (2005), *Structure-Borne Sound: Structural Vibrations and Sound Radiation at Audio Fequencies*, Springer Science & Business Media.

Dirlik, T. (1985), *Application of Computers in Fatigue Analysis*, PhD Thesis, University of Warwick.

Durant, C., Robert, G., Filippi, P.J.T., and Mattei, P-O. (2000), "Vibroacoustic response of a thin cylindrical shell excited by a turbulent internal flow: Comparison between numerical prediction and experimentation", *Journal of Sound and Vibration*, Vol.229, No.5, pp.1115-1155.

Energy Institute (2008), *Guidelines for the Avoidance of Vibration Induced Fatigue Failure in Process Pipework*, Energy Institute London.

Graber, S.D. (2010), "Manifold flow in pressure-distribution systems", *Journal of Pipeline Systems Engineering and Practice*, Vol.1, No.3, pp.120-126.

Garrison, W.G. (1988), "Major fires and explosions analysed for 30-year period", *Hydrocarbon Process* (United States), Vol.67, No. 9, pp.115-118.

Guo, B., Song, S., Chacko, J., and Ghalambor, A. (2005), *Offshore Pipelines*, Vol. 281. Elsevier, Burlington, VT

Hambric, S.A., Boger, D.A., Fahnline, J.B., and Campbell, R.L. (2010), "Structure-and fluid-borne acoustic power sources induced by turbulent flow in 90 piping elbows", *Journal of Fluids and Structures*, Vol.26, No.1, pp.121-147.

Jacobsen, F., and Juhl, P.M. (2013), *Fundamentals of General Linear Acoustics*, John Wiley & Sons

Mandhane, J.M., Gregory, G.A. and Aziz, K. (1974), "A flow pattern map for gas: Liquid flow in horizontal pipes", *International Journal of Multiphase Flow*, Vol.1, No.4, pp.537-553.

Maymon, G. (2008), *Structural Dynamics and Probabilistic Analysis for Engineers*, Elsevier.

Moussou, P. (2003), "An excitation spectrum criterion for the vibration-induced fatigue of small bore pipes", *Journal of Fluids and structures*, Vol.18, No.2, pp.149-163.

Lee, Y.L., Pan J., Hathaway., R, and Barkey, M. (2005), *Fatigue Testing and Analysis: Theory and Practice*, Butterworth-Heinemann.

Newland, D.E. (2012), *An Introduction to Random Vibrations, Spectral and Wavelet Analysis*, Courier Corporation.

Norton, M.P., and Bull, M.K. (1984), "Mechanisms of the generation of external acoustic radiation from pipes due to internal flow disturbances", *Journal of Sound and Vibration*, Vol.94, No.1, pp.105-146.

Norton, M.P. and Karczub, D.G. (2003), *Fundamentals of Noise and Vibration Analysis for Engineers*, Cambridge University Press.

Norton, M.P. and Pruiti, A. (1991), "Universal prediction schemes for estimating flow-induced industrial pipeline noise and vibration", *Applied Acoustics*, Vol.33, No.4, pp.313-336.

Peltier, L.J., and Hambric, S.A. (2007), "Estimating turbulent-boundary-layer wall-pressure spectra from CFD RANS solutions", *Journal of Fluids and Structures*, Vol.23, No.6, pp. 920-937.

Peng, L-C., and Peng, T-L. (2009), *Pipe Stress Engineering*, American Society of Mechanical Engineers.

Pigford, R.L., Ashraf, M., and Miron, Y.D. (1983), "Flow distribution in piping manifolds", *Industrial and Engineering Chemistry Fundamentals*, Vol.22, No.4, pp.463-471.

Ragan, P., and Manuel, L. (2007), "Comparing estimates of wind turbine fatigue loads using time-domain and spectral methods", *Wind Engineering*, Vol.31, No.2, pp.83-99.

Riverin, J.L., de Langre, E. and Pettigrew, M.J. (2006), "Fluctuating forces caused by internal two-phase flow on bends and tees", *Journal of Sound and Vibration*, Vol.298, No.4-5, pp.1088-1098.

Riverin, J-L., and Pettigrew, M. J. (2007), "Vibration excitation forces due to two-phase flow in piping elements", *Journal of Pressure Vessel Technology*, Vol.129, pp.7-13.

Tanaka, G., Yamaguchi, R., Liu, H., and Hayase, T. (2016), "Fluid vibration induced by high-shear-rate flow in a T-junction", *Journal of Fluids Engineering*, Vol.138, No.8, pp. 081103:1-8

Tunstall, M. J., and Harvey, J.K. (1968), "On the effect of a sharp bend in a fully developed turbulent pipe-flow", *Journal of Fluid Mechanics*, Vol.34, No.3, pp.595-608.

Wang, S., and Shoji, M. (2002), "Fluctuation characteristics of two-phase flow splitting at a vertical impacting T-junction", *International Journal of Multiphase Flow*, Vol.28, No.12, pp.2007-2016.

Wirsching, P.H., Paez, T.L., and Ortiz, K. (2006), *Random Vibrations: Theory and Practice*, Courier Corporation.

Wu, Y., Wang, R., Wang, Y. and Feng, X. (2018), "An area-wide layout design method considering piecewise steam piping and energy loss", *Chemical Engineering Research and Design*, Vol.138, pp.405-417.

Authors' Biographical Notes:

Richard Bachoo *is currently a Lecturer in the Department of Mechanical and Manufacturing Engineering at The University of the West Indies, St. Augustine. He served as a Mechanical and Piping Engineer with the international oil and gas consultancy firm, WorleyParsons for several years before returning to academia in 2017. His research interests include Flow Induced Vibration, High Frequency Structural Vibration and Probabilistic Structural Dynamics.*

Jacqueline Bridge *is currently Head and Senior Lecturer in the Department of Mechanical and Manufacturing Engineering at The University of the West Indies, St. Augustine. Her research and teaching interests are in the area of Applied Mechanics, with special emphasis on Mechanical Vibrations, Nonlinear Dynamical Systems Theory and Finite Element Methods.* ■